J Wood Sci (1998) 44:28–34

ORIGINAL ARTICLE

Takahisa Nakai · Naoyasu Igushi · Kose Ando

Piezoelectric behavior of wood under combined compression and vibration stresses I: Relation between piezoelectric voltage and microscopic deformation of a Sitka spruce (*Picea sitchensis* Carr.)*

Received: January 10, 1997 / Accepted: July 1, 1997

Abstract This study investigated the relation between piezoelectric behavior and the deformation of trachieds in real time under combined compression and vibration stresses. Scanning electron microscope images were recorded directly into a video recorder. Two types of microscopic destruction were observed in the specimens. With the first type, although a small uprush around the boundary of the annual ring was observed, the specimens were broken only by shearing fracture in the 45° direction. With the second type, the specimens were finally broken by shearing fracture after repeated buckling. In these cases the piezoelectric voltage increased almost linearly in the elastic region, proceeded to the maximal point, and then decreased gradually. Finally a clear peak appeared in the buckling and shearing fracture. There is a curved relation between the specific gravity and the piezoelectric parameter when the influence of voids is considered, and there is a linear relation between the dynamic Young's modulus and the piezoelectric parameter when the stress is considered.

Key words Combined compression and vibration stresses · Piezoelectric voltage · Buckling · Shearing fracture

T. Nakai (✉)[1]
Japan Science and Technology Corporation (JST), 4-1-8 Honmachi, Kawaguchi 322, Japan

N. Igushi
Higashiura Karimoku, 1-14 Nanei-cho, Fujie, Higashiura, Chita-gun, Aichi 470-21, Japan

K. Ando
School of Agricultural Science, Nagoya University, Furo-cho, Chikusa-ku, Nagoya 464-01, Japan

Present address:
[1]Wood Physics Laboratory, Wood Technology Division, Forestry and Forest Products Research Institute, P.O. Box 16, Tsukuba, Norin Kenkyu Danchi-nai, Ibaraki 305, Japan
Tel. +81-298-73-3211, ext. 576; Fax +81-298-73-3798
e-mail: jaja@ffpri.affrc.go.jp

*Part of this paper was presented at the 46th annual meeting of the Japan Wood Research Society in Kumamoto, April 1996

Introduction

We reported earlier[1–3] that analysis of the deformation and destruction mechanism based on the piezoelectric effect of wood is a distinctive technique that can be generally applied to crystalline insulating materials. The practical application of this method utilizing the piezoelectric effect of wood can be classified broadly into two types.

One application is to utilize wood as a piezoelectric material for industrial purposes. Regrettably, the piezoelectric constant of wood is small, approximately 10^{-14} C/N, so it is difficult to utilize wood as a piezoelectric material. However, it has recently been found that wood can show high piezoelectricity when its natural cellulose, which is a major component of wood, is transformed into a conducting form. Therefore, many studies to achieve high piezoelectricity based on cellulose and other high molecular materials are now in progress.

Another application is to use the piezoelectric effect for nondestructive evaluation of wood quality and the stress state of wood structures. The quality evaluation relies on the fact[4–7] that the piezoelectric charge density on the surface of wood and the piezoelectric voltage change greatly at weak points of wood, such as knots and pith, and are related to the physical values of the wood, such as Young's modulus and specific gravity, on which quite a few studies have already been reported. Insufficient studies have been conducted on the applicability of piezoelectricity to evaluating the stress state.

It is important to know about the structural changes of wood during deformation to clarify the deformation and destruction mechanism of wood. No definitive explanation has yet been established because the destruction mechanism of wood is complicated. Fractography, an effective technique for elucidating the mechanism of deformation and destruction, has been widely used[8,9] for estimating the progress and type of destruction. However, this technique is not suited to evaluating continuous destruction processes because it can be applied only after destruction.

In this study we attempted to observe the deformation process of wood, in particular of trachieds, in real time by recording scanning electron microscope (SEM) images directly on a video recorder. We investigated, using a nondestructive method, the relation between the deformation of tracheids and the piezoelectric behavior of the specimen to obtain fundamental information on the stress state and the prediction of strength for wood structures.

Experiments

Specimens

The specimens were made of kiln-dried Sitka spruce (*Picea sitchensis* Carr.) of cross section 15 × 15 cm and length 100 cm. The external form of the specimen shown in Fig. 1 is 0.5 × 1 × 6 cm. The arches were made on both sides of the central part of the specimen, and we set the observation plane on the radial face. In this case, the angle, (θ) between the axial direction and the fiber direction of the specimen was 45°. The moisture contents of the specimen were 5.7% and 3.5%, immediately before the specimen was fixed to the jig in the chamber of the SEM and immediately after the observation, respectively. The averaged value of specific gravities, (ϱ) of specimens before observation was 0.48. The dynamic piezoelectric modulus was reported to decrease suddenly when the moisture content of the specimen exceeded 6% because of the participation of the molecule layer of the water when the cellulose is combined with water.[10] The influence of the moisture content was ignored in this study because the moisture content was less than 6%.

As electrodes for detecting the piezoelectricity, platinum was spattered on the centers of the upper and lower surfaces of the specimen facing each other using a vacuum evaporation device (Akashi, Tokyo, Japan). The electrode was 0.5 × 2.0 cm. Silver foil, whose thickness, length, and width were 100 μm, 3 cm, and 1 mm, respectively, was used as the lead wire. The piezoelectric voltage was detected by the measuring apparatus shown in Fig. 2. Specimens were conditioned in a desiccater with P_2O_5 after vacuum-drying for 24 h.

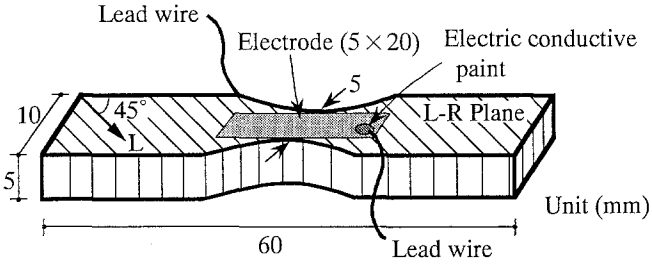

Fig. 1. Test specimens. The observation plane of the scanning electron microscope (SEM) is on the longitudenal–radial (*L–R*) plane in this study

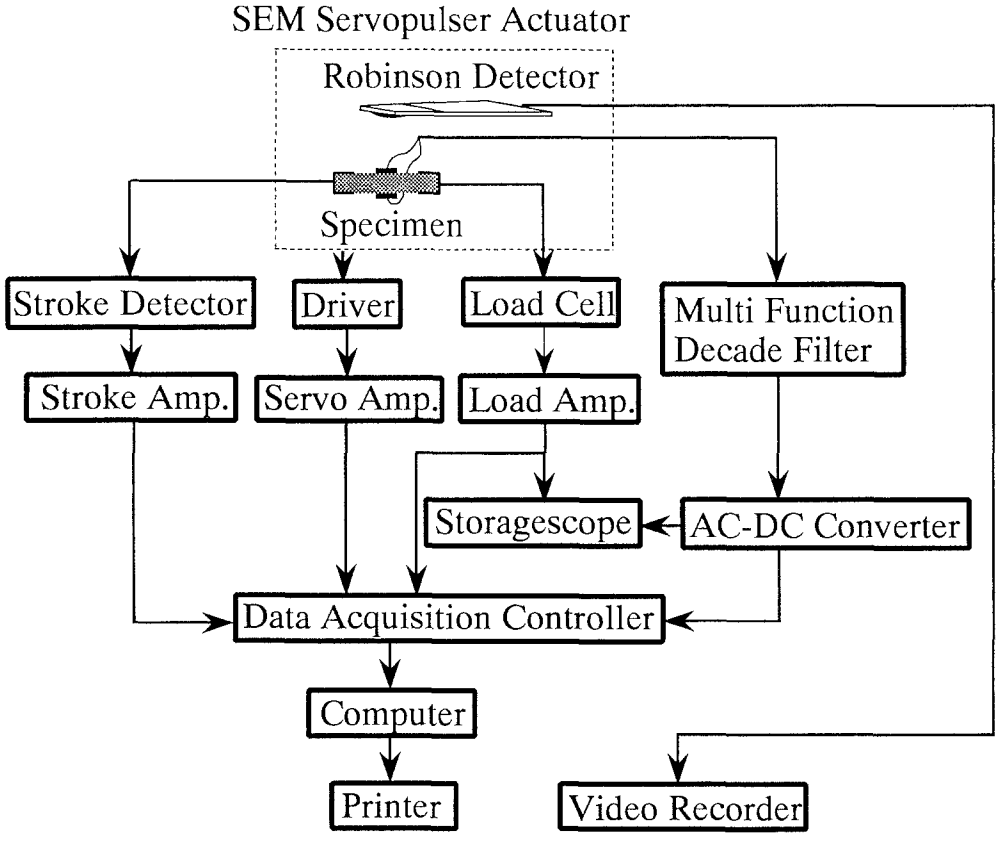

Fig. 2. Measuring system of applied load, piezoelectric voltage, and displacement of the specimen

Loading method and measurement of piezoelectric voltage

A testing machine controlled by oil pressure (Servo pulser, full scale range ±500kgf; Shimadzu, Tokyo, Japan) was used for loading. Specimens were set on the jig and loaded by a static compression load with a superimposed minute sinusoidal load (F) given by Eq. (1), below. The order of loadings was as follows: An initial load (F_0) of 2kgf was applied following by a sinusoidal load with a frequency (f) of 30Hz and an amplitude (a) of 2kgf. Finally, a static compression load with loading state, $a_0 \simeq 0.1$kgf/s was applied until the specimen failed. The sinusoidal load makes it possible to detect the piezoelectric voltage in this measuring apparatus. The combined load (F) is given by

$$F = F_0 + a\sin(\omega t) + a_0 t \quad (1)$$

where t is the time after loading, and ω is the angular velocity ($2\pi f$).

A block diagram of the measurement system of piezoelectric voltage (load, displacement) is shown in Fig. 2. The piezoelectric voltage generated by wood was detected by electrodes and amplified with removal of noise by a one-third octave bandpass filter of input impedance 10MΩ (NEC Sanei, Tokyo, Japan). It was measured with a highly sensitive alternating-current voltmeter built in to an AC-DC converter (NF Circuit Design Block, Tokyo, Japan). In this study the piezoelectric voltage determined by the measuring apparatus is an extreme value of the signal. The compression load and displacement were measured by the load cell and the stroke detector built-in SEM servopulse device. The zero point of compression displacement was set at the position of the measuring point immediately after applying the initial load. The output values of these instruments were stored simultaneously in a data acquisition controller (NEC Sanei) whose measurement speed was 100ms integral time; they were recorded by a personal computer (PC-9801vm; NEC, Tokyo, Japan).

To film the condition of the specimen during the process of compression deformation, the picture output in real time from the Robinson detector (bandwidth >5MHz, spatial resolution >10nm, useful range of accelerating voltage ≥5kV, retractable distance 63mm) in the SEM was recorded by a video recorder (Aiwa, Tokyo, Japan). The image was printed by a video printer (SCT-CP220; Mitsubishi Electric, Tokyo, Japan).

Results and discussions

Piezoelectric voltage–displacement curves corresponding to load–displacement curves and fracture of specimens

Two types of microscopic deformation were observed in this study. The difference between these two deformation processes influences greatly the relation between piezoelectric voltage, load, and displacement of the specimen.

First, typical piezoelectric voltage and load–displacement (P, L–D) curves and the form of failure are shown in Figs. 3 and 4. As shown in Fig. 3, initially the piezoelectric voltage increases proportionally with the load, and the P–D curve is convex; the piezoelectric voltage then increases suddenly and decreases suddenly when the load suddenly decreases. As shown in Fig. 4, though the small uprush around the boundary of the annual ring is observed, specimens are broken only by a shearing fracture in the 45° direction.

The other typical piezoelectric voltage, load–displacement curves and the form of failure are shown in Figs. 5 and 6. Although the peak of the convex part of the P–D curve is depressed compared with that of Fig. 3, roughly speaking the same tendency as described above is recognized in the piezoelectric voltage. The significant difference between them is that there are three clear peaks (P_1, P_2, P_3) in Fig. 5. These piezoelectric voltage peaks responded to a sudden

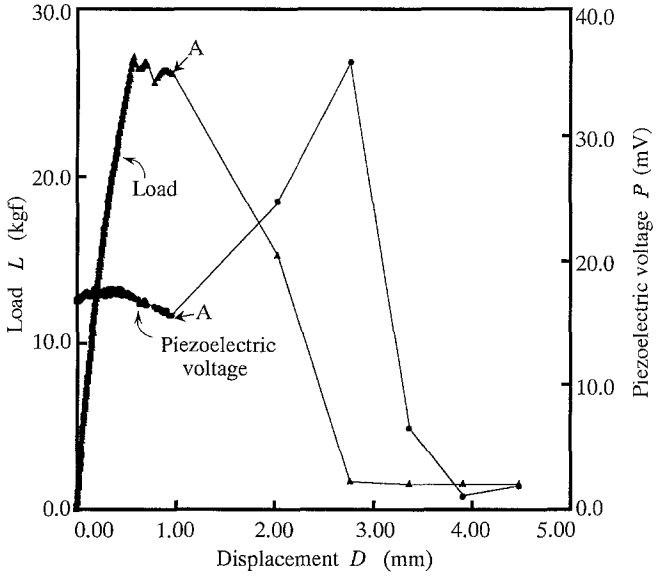

Fig. 3. Examples of piezoelectric voltage (P) and load–displacement curves. *Circles*, piezoelectric voltage; *triangles*, load; *A*, the turning point of each variable at a given period (A) of loading

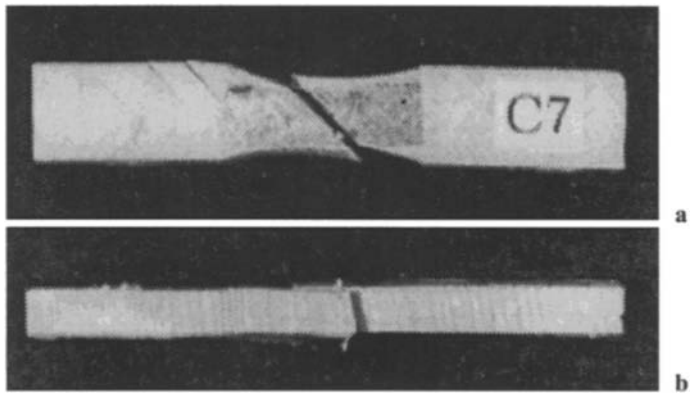

Fig. 4. Fracture type of the specimen after the test, obtained from the specimen represented in Fig. 3. **a** plan, **b** side view

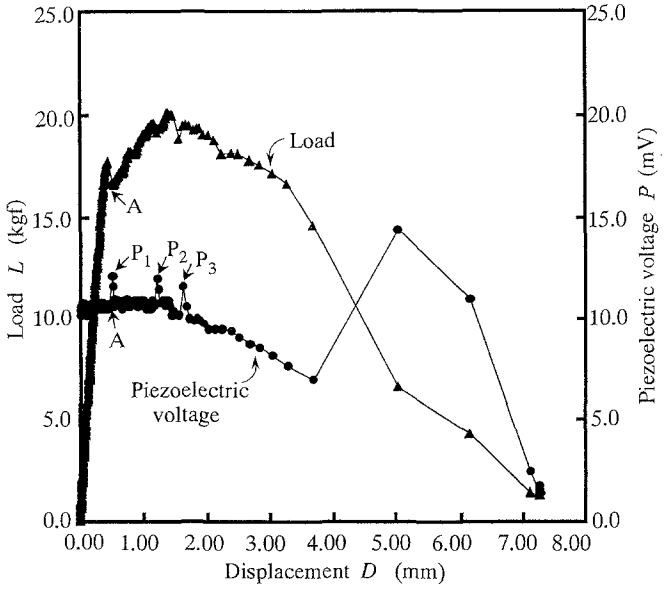

Fig. 5. Examples of piezoelectric voltage (P) and load–displacement curves. P_1–P_3 represent the piezoelectric voltage peaks generated with the buckling of the specimen

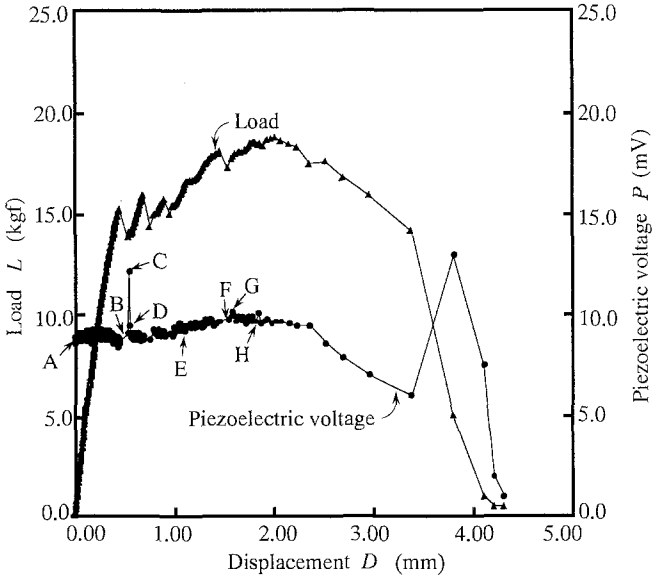

Fig. 7. Examples of piezoelectric voltage (P) and load–displacement curves. SEM images at points A–H are shown in Fig. 8

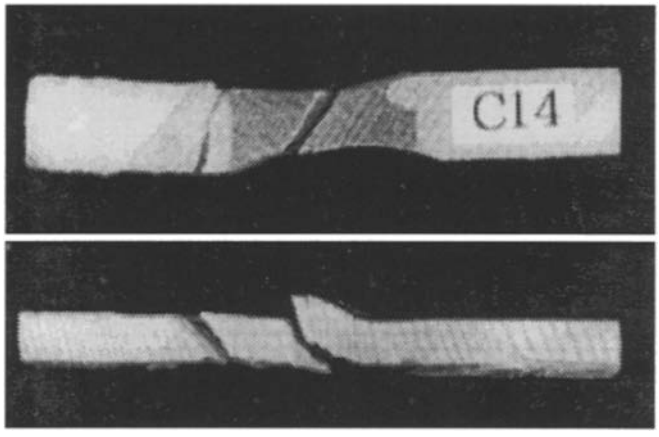

Fig. 6. Fracture type of the specimen after the test, obtained from the specimen represented in Fig. 5. **a** plan, **b** side view

drop in load with a slight delay. This point is described later in detail, but these peaks appear to be related to wrinkles on the surface of the specimen. For the sake of brevity, hereafter we refer to the uprush and wrinkle around the boundary of annual ring as "buckling" of the specimen. As shown in Fig. 6, specimens are finally broken by a shearing fracture after repeating buckling.

The relation between the P and L–D curves and the deformations of tracheids are shown in Figs. 7 and 8, which are cases when the specimen repeatedly buckled and failed by a shearing fracture. Points A to H in Fig. 7 correspond to those in Fig. 8. Point A is the state of the specimen before applying the load. Point B is where clear buckling was first observed. The load suddenly drops at this point, but a peak in the piezoelectric voltage does not appear, becoming clear a few seconds later at point C. Clear, large buckling appears for the second time at point F after the amount of buckling has increased at points D and E. Different from the case in Fig. 5, the reason for this pattern may be that the piezoelectric voltage tended to increase after the first peak. After this point the specimen breaks, and the piezoelectric voltage increases/decreases suddenly with a sudden drop in the load, as shown in Fig. 7. It follows that the piezoelectric voltage definitely responds to the deformation of the specimen–the buckling and breaking in particular.

We hypothesize that the cause of the change in piezoelectric voltage in these elastic and plastic regions is the increase of the elastic strain energy of the specimen. If the strain of crystal lattice perpendicular to the direction of the cellulose molecular chain comes to be of the same order as the macroscopic strain of specimen, as claimed by Suzuki,[11] the piezoelectric voltage generated by the hydrogen bonding in the cellulose molecular chain or among cellulose molecular chains increases in proportion to the vibration load because there is no mutual restriction among cellulose molecular chains in the elastic region. The *decrease* in piezoelectric voltage may be due to the following: In the plastic region, particularly before the buckling or breaking point, we suspect that the piezoelectric voltage decreases because the restriction of those local vibrations increases as cellulose molecular chains come close to each other.

Piezoelectric voltage at the proportional limit and its use in predicting strength

The piezoelectric voltage (P_p), load (L_p), and displacement (D_p) at the proportional limit are shown in Table 1. The

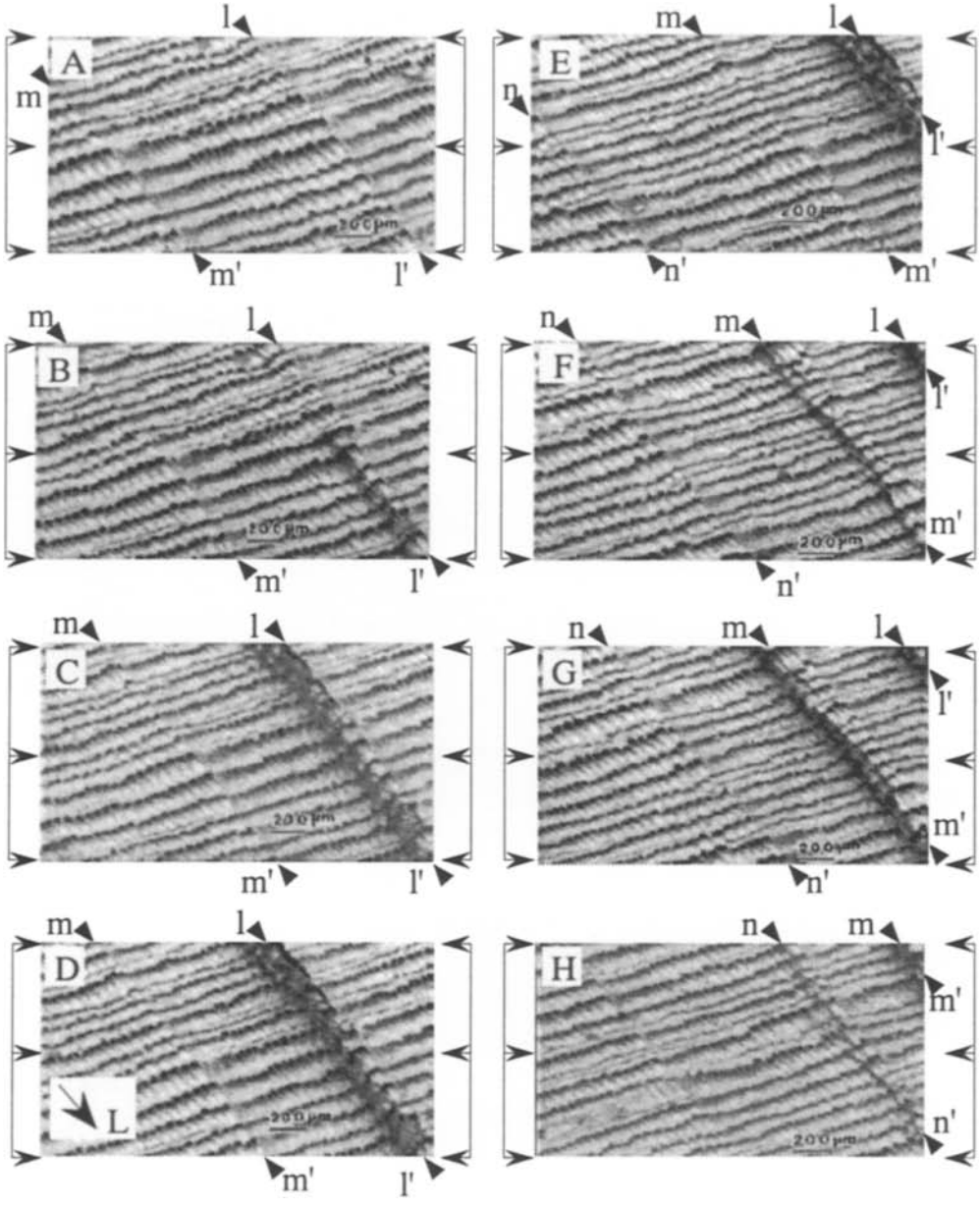

Fig. 8. Typical microscopic deformation on the L–R plane of the specimen during the combined compression and vibration test. *A–H*, see Fig. 7; *arrowheads*, loading direction; l–l′, m–m′, n–n′, annual rings. SEM image **A** shows the state of the specimen before applying the load

proportional limit is defined as the point where the regression line obtained from the regression analysis for the linear part ($0\,\text{mm} < D < 0.10\,\text{mm}$) of the *L–D* curve leaves the *L–D* curve.

Using the parameter $P_p/(\varrho \cdot L_p)$, excluding the influence of the voids in the wood and the load, where ϱ is the specific gravity, we investigated the relation between this parameter and the compressive Young's moduli (E_c) or compressive strength (*CS*) of specimens. *CS* is defined as the maximum load divided by the cross-sectional area of the specimen. The latter relation is investigated to forecast the information related to the strength of the specimen in the plastic region from the piezoelectric information in the elastic region. As shown in Figs. 9 and 10, the plotted values of $P_p/(\varrho \cdot L_p)$ corresponded to the E_c and *CS* of specimens, respectively. In both cases, linear relations are found.

$$\begin{cases} E_c\left(\times 10^3\,\text{kgf/cm}^2\right) = 1.18 \cdot \left(\dfrac{P_p}{\varrho \cdot L_p}\right) + 3.15 \\ CS\,(\text{kgf}) = 5.91 \cdot \left(\dfrac{P_p}{\varrho \cdot L_p}\right) + 27.5 \end{cases} \tag{2}$$

If the relation between *CS* and ϱ is defined by the equation[12]

$$CS = k\varrho \tag{3}$$

where k denotes the experimental constant, from the second expression of Eq. (2) and Eq. (3) the following equation is obtained:

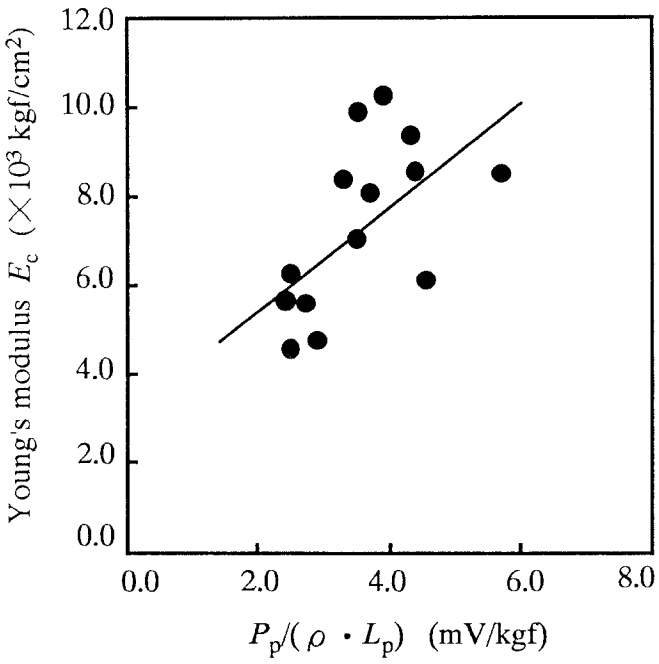

Fig. 9. Relation between Young's modulus (E_c) and $P_p/(\varrho \cdot L_p)$. P_p and L_p, piezoelectric voltage and load at proportional limit; ϱ, specific gravity; *straight line*, regression line

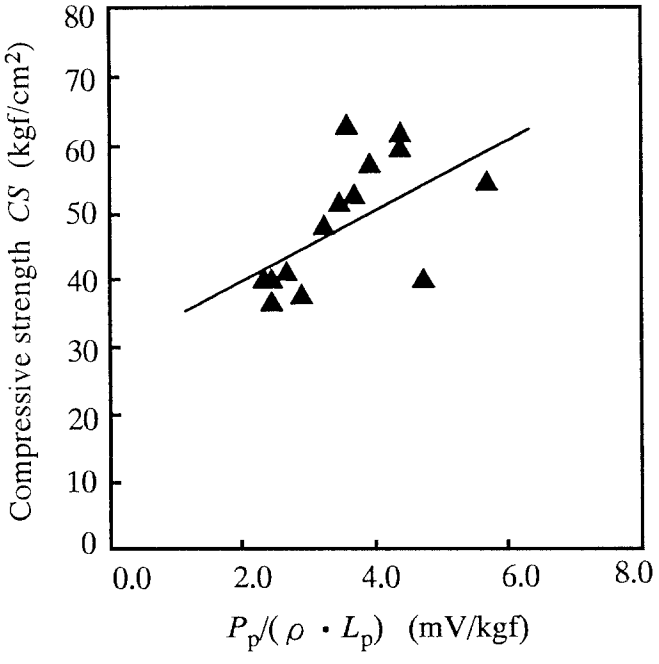

Fig. 10. Relation between compressive strength (CS) and $P_p/(\varrho \cdot L_p)$

$$
\begin{aligned}
P_p &= \mathrm{A} \cdot \varrho^2 - \mathrm{B} \cdot \varrho \\
&= L_p \left(\mathrm{A}' \cdot \varrho^2 - \mathrm{B}' \cdot \varrho\right) \\
&= const. \cdot L_p \qquad (4) \\
&\left(\mathrm{A} = \frac{k}{5.91} \cdot L_p = \mathrm{A}' \cdot L_p, \right. \\
&\left. \mathrm{B} = 4.65 \cdot L_p = \mathrm{B}' \cdot L_p, \frac{\mathrm{B}}{\mathrm{A}} \leq \varrho \right)
\end{aligned}
$$

The relation between the piezoelectric voltage under a certain load and the specific gravity is expressed by a quadratic curve that is lower convex. This result has the same tendency as Galligan's result, which found that relations between the maximum amplitude of piezoelectric voltage detected by the stress wave generated by an air-hammer and the specific gravity or the dynamic Young's modulus are, respectively, curved or linear relations.

Table 1. Results of piezoelectric voltage, load, and displacement at the proportional limit

Specimen no.	Proportional limit		
	Piezoelectric voltage (P_p) (mV)	Load (L_p) (kgf)	Displacement (D_p) (mm)
1	8.9	8.0	0.20
2	10.9	8.7	0.13
3	19.1	11.1	0.15
4	8.9	8.1	0.17
5	7.1	7.2	0.19
6	16.9	10.0	0.15
7	17.2	7.7	0.11
8	15.2	10.7	0.14
9	11.2	7.5	0.09
10	11.3	7.9	0.12
11	9.0	9.2	0.20
12	7.5	7.6	0.15
13	12.8	9.0	0.15
14	10.5	5.9	0.11
Average	11.9	8.5	0.15

Conclusions

This study investigated the relation between piezoelectric behavior and microscopic fractures of wood, in particular the deformation of tracheids, and it clarified the relation as described below.

1. Two types of microscopic deformation were observed in the specimens. With both types the piezoelectric voltage increased almost linearly in the elastic region, proceeded to the maximal point, and then decreased gradually. Finally, a clear peak appeared at the buckling and shearing fracture.

2. There is a curved relation between the specific gravity and the piezoelectric parameter when the influence of voids is considered, and there is a linear relation between the dynamic Young's modulus and the piezoelectric parameter when the stress is considered.

3. This examination, based on X-ray analysis, has helped clarify the causes of the increase and decrease in piezoelectric voltage. To further understand the relevance to the crystalline structure of woods, the dynamic behavior of woods, particularly the cellulose crystals, must be examined using an X-ray analysis device.

Acknowledgments We thank Dr. Naohiro Kuroda and Mr. Youki Suzuki of the Forestry and Forest Products Research Institute (FFPRI) for their valuable advice while conducting the experiment.

References

1. Sobue N (1990) The fundamental studies on the development of analysis method of fracture mechnisum of wood by using the piezoelectric effect (in Japanese). Report for a Grant-in-Aid for Scientific Research, Ministry of Education, Science and Culture (no. 01560182), pp 1–42
2. Nakai T, Takemura T (1993) Piezoelectric behaviors of wood during compression tests (in Japanese). *Mokuzai Gakkaishi* 39(3):265–270
3. Nakai T, Suzuki Y, Igushi N, Ando K (1996) The piezoelectric behaviors during fracture process of wood (in Japanese). In: Abstracts of 46th Annual Meeting of the Japan Wood Research Society, Japan Wood Research Society, Tokyo, pp 87
4. Galligan WL, Bertholf LD (1963) Piezoelectric effect in wood. Forest Prod J 13:517–524
5. Knuffel WE, Pizzi A (1986) The piezoelectric effect in structural timber. Part I. Holzforshung 40:157–162
6. Knuffel WE (1988) The piezoelectric effect in structural timber. Part II. Holzforshung 42:247–252
7. Smetana JA, Kelso PW (1971) Piezoelectric charge density measurements on the surface of Douglas-fir. Wood Science 3:161–171
8. Furukawa I (1980) Studies on the fractographic features of the longitudinal tensile fracture of coniferous woods (in Japanese). Bull Tottori Univ Forest 12(Jan):83
9. Nobuchi T, Saiki H (1986) The researches on the fracture processes and fracture profiles of woods and wood composite materials (in Japanese). Report for a Grant-in-Aid for Scientific Research, Ministry of Education, Science and Culture (no. 60302083), pp 7–34
10. Uemura T (1960) Dielectric properties of woods as the indicator of the moisture (in Japanese). Ringyo Shikenjo Hokoku 119: 135
11. Suzuki M (1968) Mechanical deformation of crystal lattice of cellulose in Hinoki wood (in Japanese). Mokuzai Gakkaishi 14: 268–275
12. Asano I (1993) Mokuzai no jiten (in Japanese). Asakura Shoten, Tokyo, p 187